J Mater Sci: Mater Med (2010) 21:73–80
DOI 10.1007/s10856-009-3848-4

Structural investigation of PEG-fibrinogen conjugates

Ilya Frisman · Ron Orbach · Dror Seliktar · Havazelet Bianco-Peled

Received: 3 May 2009 / Accepted: 4 August 2009 / Published online: 20 August 2009

Abstract Controllable bio-synthetic polymeric hydrogels made from fibrinogen-poly(ethylene glycol) adducts have been successfully employed in tissue engineering. The structural consequences of PEG conjugation to fibrinogen (i.e., PEGylation) in such a hydrogel network are not fully understood. The current investigation details the structural alterations caused to the reduced fibrinogen polypeptides by the covalent attachment of linear or branched PEG chains. The structure of PEGylated fibrinogen polypeptides were comprehensively characterized using small angle X-ray scattering, light scattering, and cryo-transmission electron microscopy. These characterizations concur that the bio-synthetic hybrids self-assemble into elongated objects, having a protein core of about 50 Å in diameter decorated with multiple PEG chains. Conjugates with branched PEG chains were shorter, and have lower average molecular weight compared to conjugates with linear chains. The diameter of the protein core of both samples was similar, suggesting a tail-to-head aggregation of the PEGylated fibrinogen polypeptide. A more complete understanding of this unique structural arrangement can provide further insight into the full extent of biofunctional accessibility in a biomaterial that combines the advantages of synthetic polymers with bioactive proteins.

I. Frisman · H. Bianco-Peled (✉)
Department of Chemical Engineering, Technion-Israel Institute of Technology, Haifa 32000, Israel
e-mail: bianco@tx.technion.ac.il

R. Orbach
The George S. Wise Faculty of Life Science, Tel-Aviv University, Tel Aviv 69978, Israel

D. Seliktar
Department of Biomedical Engineering, Technion-Israel Institute of Technology, Haifa 32000, Israel

D. Seliktar · H. Bianco-Peled
The Russell Berrie Nanotechnology Institute, Technion-Israel Institute of Technology, Haifa 32000, Israel

1 Introduction

Covalent attachment of synthetic polymers to biological macromolecules offers an effective means to modify their properties, providing enhanced functionality for drug delivery and tissue engineering. One of the common approaches to achieve this goal is the covalent attachment of poly (ethylene glycol) (PEG) to therapeutic proteins, termed PEGylation. Macromolecular drugs have been successfully PEGylated to decrease their recognition by the host immune system. Likewise, PEGylation of therapeutic proteins is known to alter degradation rate by proteolytic enzymes, thus prolonging circulation half-life, reducing renal filtration, and altering biodistribution by increasing apparent molecular weight [1]. PEGylation has also been employed in biomaterial design wherein synthetic polymer networks are decorated with multiple polypeptides for enhanced bioactivity. For example, PEG hydrogels were created with PEGylated cell-adhesion-promoting proteins like fibronectin, laminin and fibrinogen [2–4]. These bioactive and structurally versatile hydrogels were successfully employed as scaffolds in tissue engineering [3, 5]. The protein backbone of these materials provides cell attachment sites and inherent biodegradability, whereas the PEG provides mechanical strength and physicochemical flexibility. Therefore, bio-synthetic scaffolds employing a PEGylated protein design strategy can offer better control over cell-biomaterial interactions.

Before taking full advantage of a PEGylated protein biomaterial to precisely regulate cell-biomaterial

interactions, it is important to understand the structural alteration to the protein caused by large-scale PEGylation. Biomaterials made through PEGylation may contain multi-PEGylated protein macromolecules with unique tertiary and quaternary conformations that are prescribed by the complex molecular interaction between the protein backbone and the PEG side chains. The conformational restructuring of the bioactive moieties in the material may significantly affect their overall bioactivity [6, 7]. It stands to reason that the loss of biological activity in a PEGylation protein biomaterial is, at least in part, a consequence of altering the protein's native structure due to the PEG conjugation. Indeed, recent computer modeling [8] and small-angle X-ray scattering studies [9] detected changes in the 3-D structure of PEGylated hemoglobin. Yet, the structure-function of PEGylated proteins in biomaterials are poorly understood and have not received much research attention.

The current study provides an in-depth structural characterization of PEG-fibrinogen conjugates (PF). These conjugates are prepared using Michael-type addition of thiols to acrylate-functionalized PEG, and were previously studied for tissue engineering applications [2, 3, 5, 10–12, 14–20]. The reaction involves denaturation of the protein in concentrated urea solution, followed by cleavage of the disulfide bonds which separates the protein into three polypeptides. PEG-diacrylate chains are then covalently attached to the thiol groups on the protein backbone, and finally the urea is dialyzed out. Cell-seeding experiments have shown that the PEGylated product can be formed into a hydrogel that exhibits cell adhesion capabilities, suggesting that some functional aspects of the native structure of the protein are at least partially restored upon removal of the urea [3, 5, 10–14]. Nevertheless, the extent of re-folding is currently unclear. Moreover, variations in the molecular weight of the PEG and in the PEG/fibrinogen weight ratio were shown to have an effect not only on the physical properties of the hydrogels, but also on their enzymatic degradability and their interactions with cells [3, 5]. Clearly, parameters such as molecular weight and weight ratio of the constituents may significantly affect the structure of the molecular backbone of the hydrogel. Therefore, a quantitative understanding of the nano-structure of PEG-fibrinogen conjugates is critical to their successful implementation as biofunctional materials in tissue engineering.

2 Experimental section

2.1 Materials and methods

PEGylation of fibrinogen was performed according to protocols previously described [3, 5]. Briefly, 7 mg/ml of bovine fibrinogen (Aldrich, Sleeze, Germany) was dissolved in 150 mM phosphate buffered saline (PBS) containing 8 M urea. Tris (2-carboxyethyl) phosphine hydrochloride (TCEP) (Sigma-Aldrich) was added to the fibrinogen solution at a molar ratio of 1.5:1 TCEP to fibrinogen. After dissolution, the pH of the solution was adjusted to 8 using a 1 M NaOH solution. A solution of PEG-diacrylate (280 mg/ml) (Tissue Regeneration Lab., Biomed. Eng. Dep., Technion, Israel) in 150 mM PBS with 8 M urea was added and reacted for 3 h at room temperature in the dark. After the reaction was complete, the PEGylated protein was diluted 1:1 with 150 mM PBS containing 8 M urea, and precipitated by adding four volumes of acetone (Frutarom, Haifa, Israel) at room temperature in a separation funnel. The precipitate was redissolved, homogenized and dialyzed against 150 mM PBS at 4°C for 24 h with two changes of PBS. Samples for small angle neutron (SANS) experiments were prepared by exchanging the aqueous buffer with deuterium oxide-based buffer (Sigma-Aldrich) during the dialysis.

To determine the concentration of the PEGylated fibrinogen (PF), a 0.5 ml solution of the product was lyophilized overnight and weighted. The PBS salt concentration (9.8 mg/ml) was subtracted to obtain the net weight of the PF product. Next, the protein content was determined using a BCA^{TM} assay (Pierce Biotechnology, Inc., Rockford, IL), and the protein concentration was subtracted from the total PF concentration to give the PEG concentration. The PEGylation ratio was calculated based on the protein and PEG concentrations. The theoretical PEG to fibrinogen molar ratio was calculated assuming 29 attachment sites for every molecule of fibrinogen (166 kDa) [3]. Thus, (PEGylation ratio) = (fibrinogen concentration) * (theoretical PEG to fibrinogen ratio)/(PEG concentration).

2.2 Static light scattering (SLS)

SLS measurements were performed using a BI-200SM Research Goniometer System (Brookhaven Instruments Corp.). A Compass 415 M solid-state laser (Coherent) was used to generate monochromatic green light of 532 nm wavelength. The detector assembly included a selected photomultiplier tube (PMT), a dynode chain, and an integral amplifier/discriminator. The BI-9000AT digital signal processor was used as a photon counter. The experiments were performed at constant temperature of 25°C. Samples were placed in a glass cell and immersed in a glass vat containing decalin as the index matching fluid. The measurement gives the value of the excess time-average scattered light intensity also termed excess Rayleigh ratio, ΔR_θ. Windows-based Zimm Plot software Version 3.17 provided with the instrument was employed for data processing. The calculation was based on Eq. 1 that relates ΔR_θ to the

weight-average molecular weight of a polymer in dilute solution, $\overline{M}_w$, [21, 22]:

$$\frac{K*c}{\Delta R_\theta} \approx \left(1/\overline{M}_w\right) * \left[1 + \frac{1}{3} * \left\langle R_g^2 \right\rangle * q^2\right] + 2A_2 * c \qquad (1)$$

where K is an optical constant, c is the polymer concentration (g mL^{-1}), R_g is the average radius of gyration, $q = 4\pi * n * \sin(\theta)/\lambda$ is the scattering vector, n is the refractive index of the medium, 2θ is the scattering angle, λ is the wavelength of the incident beam on vacuum, and A_2 is the second virial coefficient. A plot of $K*c/\Delta R_\theta$ against $\sin^2(\theta) + k*c$ (where k is an arbitrary constant) known as a Zimm plot, was used to obtain the values of $\overline{M}_w$, R_g, and A_2. The refractive index increment, *dn/dc*, was measured separately for each sample using a differential refractometer BI-DNDC (Brookhaven Instruments).

2.3 Small angle X-ray scattering (SAXS)

SAXS measurements were performed using a slit-collimated compact Kratky camera (A. Paar Co.). The entrance slit to the collimating block was 40 μm, and the slit length delimiters were set at 15 mm. Ni filtered CuKα radiation was generated by a sealed tube (Philips). Samples were placed in mark-tubes made of quartz with wall thickness of 0.1 mm and a 2 mm path length (Hilgenberg GmbH, Germany) and their temperature was kept constant at 25°C by means of a temperature controller (A. Paar Co.). The sample to detector distance was 26.4 cm, and the flight path was kept under vacuum. Scattering was measured with a linear position sensitive detector system (Raytech, gold-coated tungsten wire in a stream of 90% Ar +10% CH_4 gas at 3 bar), with pulse-height discrimination and a multichannel analyzer (Nucleus). A total of 3000 or more counts for all channels were collected in order to obtain a low noise to signal ratio. Data was processed using primary data handling (PDH) software. To place the data on an absolute scale, corrections were made for detector efficiency, the presence of background radiation and the scattering of the empty cell. To rectify the effects of the beam dimensions, a desmearing procedure was performed according to the Indirect Transformation Method [23], using the GIFT program. Data analysis was based on fitting the SAXS to a theoretical model. Small angle scattering data were recorded from solutions at 3.17 and 21.75 mg/ml. The intensity was normalized by the concentration.

2.4 Small angle neutron scattering (SANS)

SANS experiments were carried out on LOQ diffractometer at the ISIS research center in Rutherford Appleton Laboratory, Chilton, UK. Liquid samples were placed into cylindrical quartz cuvettes (Optiglass—Starna, UK) with dimensions of 22 × 4.5 mm, 0.56 ml nominal volume and 2 mm path length. Hydrogel samples were placed in aluminum wraparounds. The sample cells were placed into two 9-position racks, which were connected to computer-controlled sample changer. The changer was linked to controlled water/oil bath and kept at a constant temperature of 25°C.

2.5 Circular dichroism

Circular dichroism (CD) spectra were recorded with an AVIV 202 spectropolarimeter (Aviv Instruments, Lakewood NJ) equipped with a temperature-controlled cell using a cell of path length 1 cm; the bandwidth was 1 nm, and the averaging time was 4 s for each measurement. Four samples were chosen for CD analysis, including: PF precursor solutions made with 10 and 20 kDa PEG; fibrinogen and PEG solutions (without the PEGylation reaction) at the same weight composition as the PF precursor solutions.

2.6 Transmission electron microscopy

Transmission electron microscopy (TEM) micrographs were obtained from ultra-fast cooled vitrified cryo-TEM specimen prepared under controlled conditions of 25°C and 100% relative humidity as described elsewhere [24]. Specimens were examined in a Philips CM120 cryo-TEM operating at 120 kV, using an Oxford CT3500 cooling-holder system that keeps the specimens at about −180°C. Low electron-dose imaging was performed with a Gatan Multiscan 791 CCD camera, using the Gatan Digital Micrograph 3.1 software package.

3 Results and discussion

We examined fibrinogen conjugated to linear and branched PEG, referred to as PF_L and PF_B, respectively. Figure 1 displays the desmeared background-subtracted SAXS curves for these samples, normalized with respect to the solution concentration. For both PF_L and PF_B, the data from two different concentrations collapses into a single curve, thus indicating that the solutions were in the dilute regime. The q^{-1} power law observed at low q values was indicative of the presence of long rod-like objects. Therefore, quantitative analysis was performed by fitting the experimental SAXS data to a model of cylinders having a length-to-radius ratio (L/R) of more than 10, for which the scattering intensity is given by [25]:

$$I(q) = n_{cyl} * \Delta\rho^2 * \left[\frac{2B_1(q*R)}{q*R}\right]^2 \left(\frac{2Si(q*L)}{q*L} - 4\frac{\sin^2(q*L/2)}{(q*L)^2}\right) \qquad (2)$$

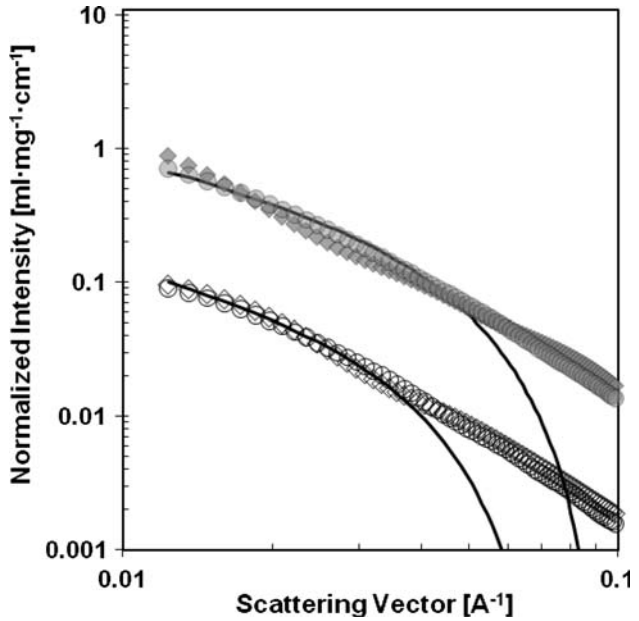

Fig. 1 Desmeared SAXS intensities normalized with respect to the samples' concentrations, from *open circle* PF_L 21.75 mg/ml, *open diamond* PF_L 3.17 mg/ml, *filled circle* PF_B, 21.75 mg/ml and *filled diamond* PF_B 3.17 mg/ml. Data for PF_B were multiplied by 10 for better visualization. The *solid line* was calculated from Eq. 2 using the best-fit parameters summarized in Table 1

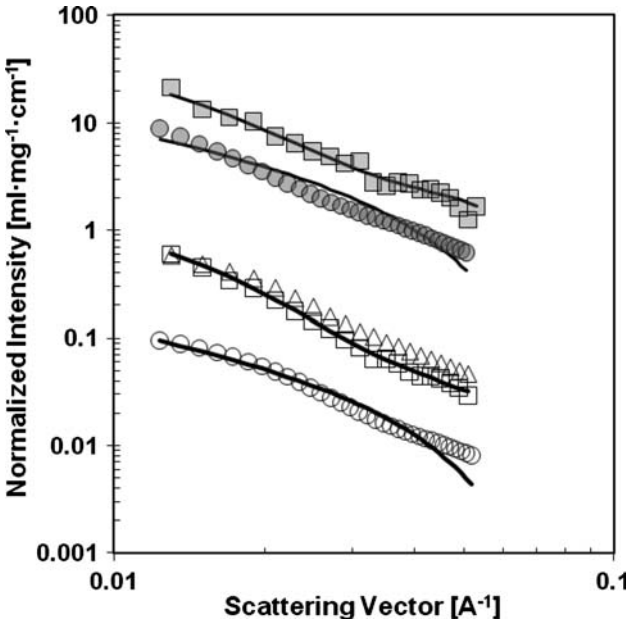

Fig. 2 SANS and SAXS curves, normalized with respect to the samples' concentrations, for PF dilute solutions. *Open circle* PF_L, 1 mg/ml, SAXS, *open square* PF_L, 1 mg/ml, SANS, *open triangle* PF_L, 3 mg/ml, SANS, *filled circle* PF_B, 1 mg/ml, SAXS, *filled square* PF_B, 1 mg/ml, SANS. Data for PF_B was multiplied by 10 for better visualization. The *solid lines* were calculated from Eq. 3 using the best-fit parameters summarized in Table 2

where n_{cyl} is the number of cylinders per unit volume, $\Delta\rho$ is the electron density difference between the cylinder and the medium, R and L are radius and the length of the cylinder, respectively, $B_1(x)$ is a Bessel function of the first order and $Si(x) = \int_0^x t^{-1}\sin(t)dt$. Preliminary attempts to fit Eq. 2 to the experimental data have shown that for very long cylinders ($L > 1500$ Å) the sensitivity of the model to L was very low. Therefore we fixed the value of L to 2000 Å. The best fits to Eq. 2, shown as solid lines in Fig. 1, were calculated from the best-fit parameters summarized in Table 1. The selected model showed a good fit to the experimental data at low values of the scattering vector. The inconsistency at high q values could be the result of polydispersity of the cylinders sizes, which was not taken into account in the model. The chosen values of the fitted parameters ensured that the condition of length-to-radius rate was fulfilled.

The SAXS curves only reflect the contribution of the fibrinogen backbone and not that of the attached PEG chains because the electron density of PEG (9.44 * 10^{-6} $Å^{-2}$) is almost identical to that of the solvent (water, 9.43 * 10^{-6} $Å^{-2}$). Contrarily, SANS experiments provided large contrast between PEG and D_2O, thus allowing for a more detailed structural analysis of the two constituents of the polymer network. Neutron scattering data of PF solutions at low concentrations is shown in Fig. 2. Based on the SAXS analysis, the fibrinogen backbone of the conjugates was depicted as a long cylindrical particle. The SANS data was therefore fitted to a model of long cylinders with attached PEG chains. This model was originally developed by Pedersen et al. [25–27] for dilute suspension of block copolymer micelle with cylindrical geometry, and later modified by Dror et al. [28] for polymers dispersing single-walled carbon nanotubes, where the size of the carbon nanotube (core) is not correlated with the size of the attached polymer chains (shell). The scattering intensity for the latter is given by:

$$I(q) = n_{cyl}[(\Delta\beta_{core})^2 F_{core}(q) + N_{chain}^2(\Delta\beta_{chain})^2 F_{chain}(q) + 2N_{chain}(\Delta\beta_{core})(\Delta\beta_{chain})S_{core-chain}(q) + N_{chain}(N_{chain}-1)(\Delta\beta_{chain})^2 S_{chain-chain}(q)] \quad (3)$$

Eq. 3 deconvolutes the scattering from the particle into four terms describing the contributions of the form factor of the cylindrical core (F_{core}), the form factor of the attached chains (F_{chain}), the cross-term between the core and chains $S_{core\text{-}chain}$, and the cross term between the chains

Table 1 Fitted parameters for a model of long cylindrical particles

Parameter	PF_L	PF_B
n_{cyl}	5.1E-2	2E-1
R	52.8 Å ± 2.66	51.3 ± 16 Å
$\Delta\rho$	2.508E-7 $Å^{-2}$	2.508E-7 $Å^{-2}$

Table 2 Fitted parameters of a model of long cylindrical particle with attached Gaussian chains

Parameter	PF_L	PF_B
n_{cyl}	7E-2	2.4E-1
R	54 Å ± 13	51 Å ± 16
N_{chain}	23 ± 4	7.3 ± 1.2
R_g *of Gaussian chain*	10 Å ± 1.5	15 Å ± 2
d	3.9	4.7
$\Delta\rho$	6.82E-6 $Å^{-2}$	4.19E-6 $Å^{-2}$

$S_{chain\text{-}chain}$. N_{chain} is the number of polymer chains attached to one cylinder, $\Delta\beta_{chain}$ and $\Delta\beta_{core}$ are the total excess scattering lengths of the cylindrical core and of the PEG chains, respectively. The polymer chains are assumed to be Gaussian, uniformly distributed on the core's surface, and monodispersed. The remoteness of the center of mass of the random coil chain from the cylinder surface is given by dR_g, where d is a constant and R_g is the radius of gyration of the PEG chain. The detailed expressions for each term can be found elsewhere [28]. The best fits to Eq. 3, shown as solid lines in Fig. 2, were calculated from the parameters summarized in Table 2. The fitting was performed simultaneously to the SANS and the SAXS curves from the same sample. We fixed the scattering length and electron densities of PEG chain to the calculated values of 1.37E-8 and 5.78E-7 $Å^{-2}$, respectively, and the length of the cylinder to 2000 Å. The values of the fitted parameters (Table 2) ensured that the condition of length-to-radius rate was fulfilled. The radius of the cylinder R obtained from the fit to Eq. 3 was similar to the one evaluated from the analysis of the SAXS data (Table 1).

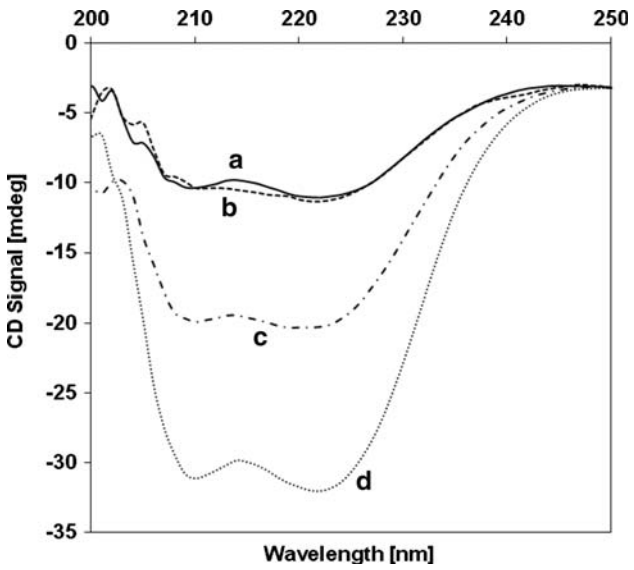

Fig. 3 CD spectrograms of 0.26 μM solutions of **a** PF with 10 kDa PEG (*solid*), **b** FP with 10 kDa PEG (*dot*), **c** PF with 20 kDa PEG (*dash-dot*), **d** FP with 20 kDa PEG (*dash*)

Fibrinogen is composed of three polypeptides α, β and γ. Each polypeptide carries between eight and ten thiol groups that provide attachment sites for the PEG chains. The total length of fibrinogen in its native conformation is about 475 Å [29]. Clearly, the small angle scattering data detected much longer cylinders, suggesting that the three PEGylated polypeptides do not fold back into the native conformation. This speculation was verified by the circular dichroism (CD) analysis of the secondary structure of PEGylated fibrinopeptide and unmodified fibrinogen (FP) solutions with added PEG chains at the same molecular weight and concentrations as the modified ones. The CD spectrograms, presented in Fig. 3, show the existence of CD signal peaks at 209 and 222 nm wave lengths at all samples.

The comparison with the literature revealed that the relevant secondary structure at these peaks belongs to the protein that contains both α-helix, β-sheet and random coil conformations [30]. The distribution of percentage of different conformation types was received from the same literary source, which reveals 34% α-helix, 28% β-sheet and 32% random coil structures for native fibrinogen. The existence of the same peaks for the PEGylated fibrinopeptides and unmodified fibrinogen may indicate that the chemical modification does not have much influence on the secondary structure of the proteins. Consequently, this may explain the positive biological interaction between the cells and the biosynthetic scaffold, even though the protein undergoes denaturation during its chemical treatment. The CD data contradicted the small angle scattering data, which detected much longer cylinders from PF solution, than the native fibrinogen molecule. However, the difference in the length scale may be relevant to the change in the tertiary protein structure, which cannot be specified by CD analysis alone.

Although the scattering objects are very long, the limitations of small angle scattering techniques do not allow determination of the exact length. Therefore we employed light scattering to determine the overall size of the cylinders. Table 3 summarizes the weight average molar mass, M_w, and the radius of gyration of the particles $R_{g,p}$ as obtained from the Zimm plot analysis. Figure 4 demonstrates a typical Zimm plot for PF_L. The molecular weights in Table 3 are compared to the average molecular weight of PEGylated polypeptide $M_{w,pp}$. The latter represents an average value for the three polypeptides, which was

Table 3 Summary of the values obtained from Zimm plots

	M_w (kDa)	$M_{w,pp}$ (kDa)	N_{agg}	$R_{g,p}$ (nm)
PF_L (PBS)	3.2E+03	1.75E+02	18	192 ± 32
PF_L (Urea)	3.0E+02	1.75E+02	1.7	48 ± 1.3
PF_B (PBS)	1.3E+03	2.66E+02	5	91 ± 6.3
PF_B (Urea)	9.1E+02	2.66E+02	3	74 ± 2.6

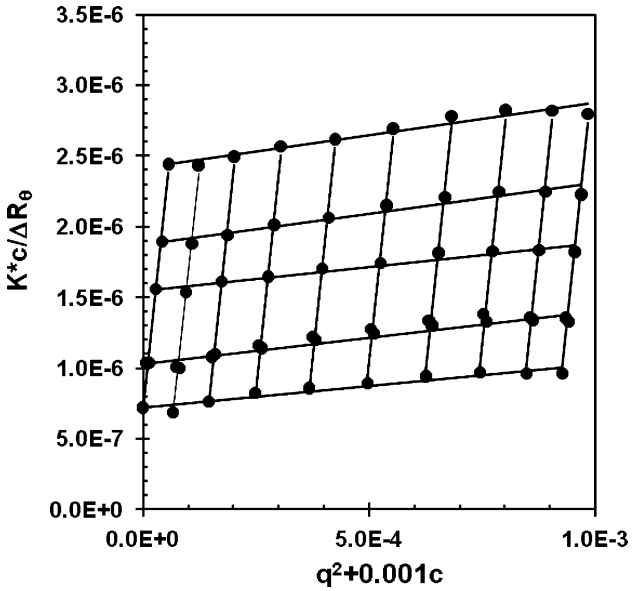

Fig. 4 Zimm Plot for PF_L in 8 M Urea solution

calculated from the PEGylation degree, the molecular weight of the PEG chains and the molecular weight of the fibrinogen sub-chains. For both PF samples, the experimental molecular weight was much higher than that of the PEGylated polypeptide. A possible reason for the high molecular weight could be intramolecular aggregation due to non-specific protein-protein interactions. Such interactions can be diminished by adding urea, which is known to screen intramolecular hydrogen bonds in proteins and solvates the hydrophobic residues [31]. In order to assess the hypothesis that the aggregation is induced by intramolecular forces, we repeated the SLS measurements with conjugates solubilized in concentrated urea solution. Indeed, both the molecular weight and the radius of gyration of PF in urea solution were lower in comparison to the same sample in PBS. The addition of urea reduced the aggregate size but did not eliminate them completely, suggesting that the protein-protein interaction was not the only mechanism involved in the aggregation.

The ratio between the experimental molecular weight and the average molecular weight of PEGylated polypeptide provides an estimate to the aggregation number, i.e., the number of PEGylated sub-chains that form a larger aggregate. Table 3 shows that the aggregation number of PF_L was much larger than that of the PF_B. Additionally, the aggregation number for PF_L solutions in PBS was almost ten-fold larger than the aggregation number in urea solution. Contrarily, the difference between the aggregation number of PF_B in PBS and in urea solution was much smaller. A possible explanation could be that the steric repulsions caused by the branched PEG chains were more effective in hindering protein–protein aggregation. Because the aggregates formed in the PF_B solutions in buffer were

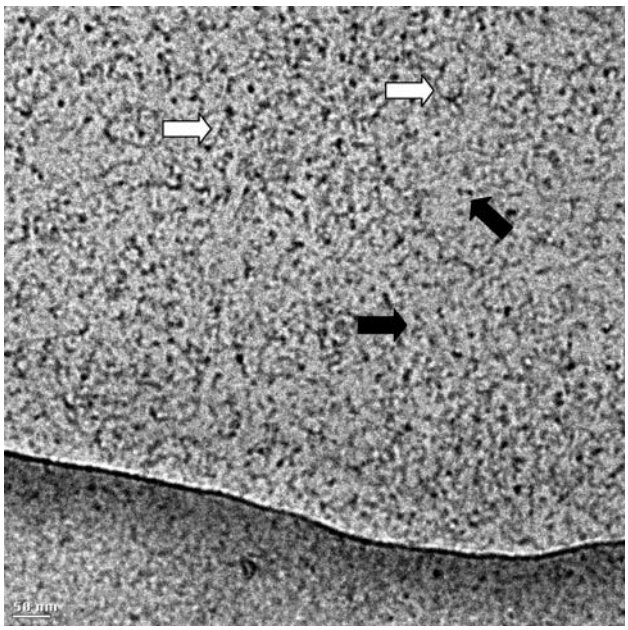

Fig. 5 Cryo-TEM image of the PF_L precursor solution. The *arrows* indicate the serpentine formations of PEG-Fibrinogen precursor molecules: *white arrows—long cylinders*, *black arrows—short cylinders*. Bar = 50 nm

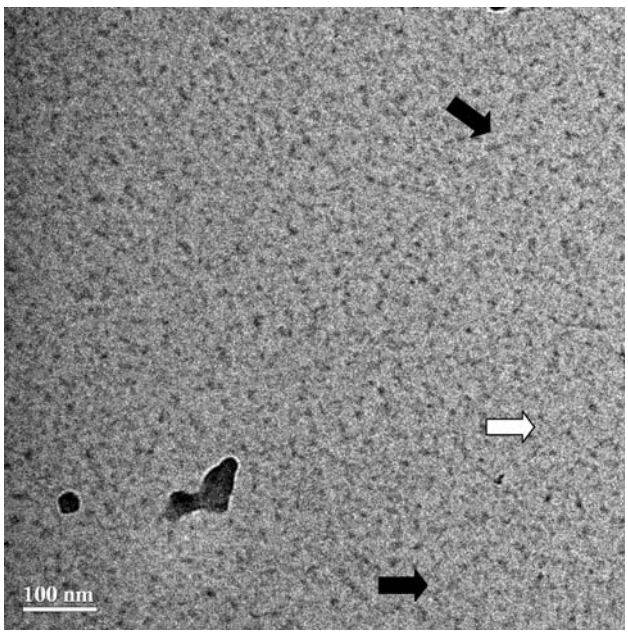

Fig. 6 Cryo-TEM image of the PF_B precursor solution. The *arrows* indicate the serpentine formations of PEG-Fibrinogen precursor molecules: *white arrows—long cylinders*, *black arrows—short cylinders*. Bar = 100 nm

smaller compare to the ones formed in PF_L solutions, the influence of adding urea to break up the aggregates was smaller.

Cryo-TEM micrographs (Figs. 5 and 6) verify the presence of elongated, serpentine objects. The length scales

of these objects are varied; from short cylinders (marked with black arrows in Figs. 5 and 6) co-exist with very long objects spanning several hundreds of nm in length (white arrows). In general, the PF_B cylinders appeared shorter when compare to PF_L cylinders, supporting the previous assumption that the branched PEG is more effective in preventing protein aggregation.

Based on the results presented above, we propose a structural model to describe the arrangement of the PEGylated polypeptides. The small angle scattering data and the cryo-TEM micrographs point out that the polypeptides self-assemble into elongated objects, with a protein core of about 50 Å in radius. The PF_B aggregates are shorter, and have lower average molecular weight; however, the diameter of the protein core of both samples was similar. This may indicate a tail-to-head aggregation of the PEGylated polypeptide. From the SANS data, one can estimate aggregation numbers of 2.4 and 1.2 per 2000 Å for the PF_L and PF_B, respectively. The corresponding aggregation numbers calculated from the SLS data were 17 and 5 for the PF_L and the PF_B, respectively. In principle, comparing the SANS and the SLS data could be used to estimate the cylinder size, however, we did not attempt to perform this calculation because it is well known that SANS and SLS are sensitive to different length scales [32, 33].

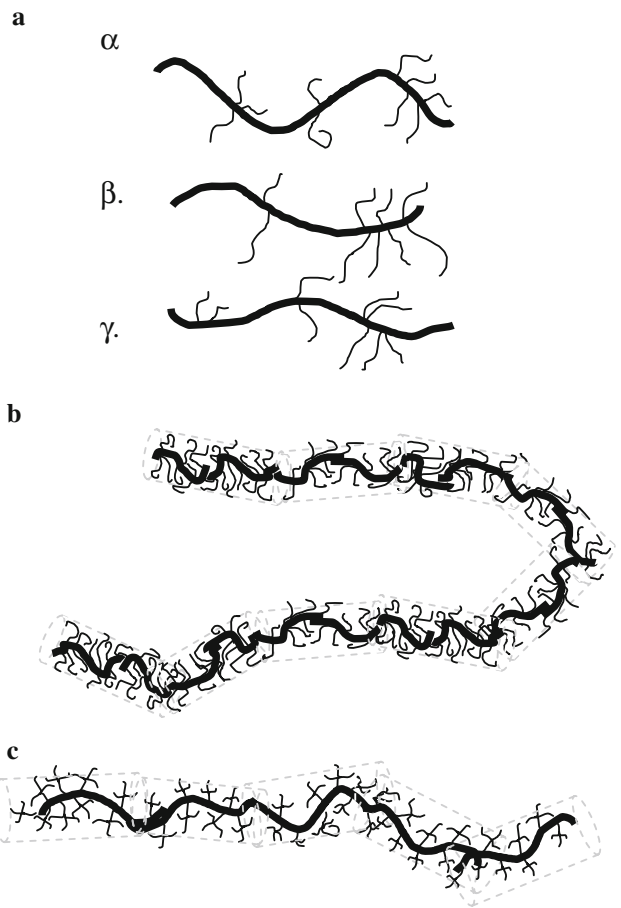

Fig. 7 Schematic representation of **a** PEGylated polypeptides, **b** PF_L aggregates and **c** PF_B aggregate

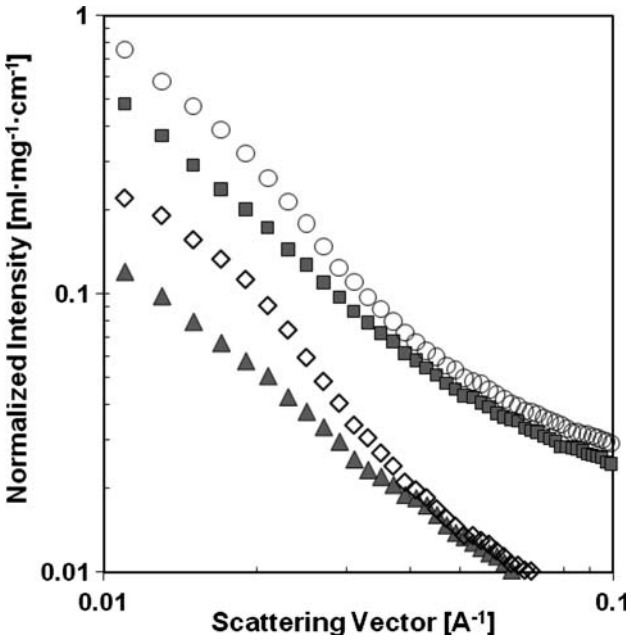

Fig. 8 SANS intensities from *open circle* PF_L gel, *filled square* PF_B gel, *open diamond* PF_L solution, *filled triangle* PF_B solution. Solutions had concentration of about 22 mg/ml

Figure 7a shows a schematic representation of the PEGylated polypeptides. We note that the thiol groups are located at the backbone ends and are not evenly distributed along the surface. It is likely that the exposed PEG-free residues allow intimate protein-protein interaction which induce formation of PF_L (Fig. 7b) and PF_B (Fig. 7c).

The analysis of scattering data from concentrated solutions requires introduction of models that will take into account inter-aggregate interaction and is beyond the scope of this work. Here we only present the raw data from concentrated solutions of PF_L and PF_B, and gels prepared *via* photo-crosslinking of solutions having the same concentrations (Fig. 8). A qualitative comparison between scattering curves shows that the scattering intensity from the hydrogels was higher compare to the solution, which could be due to inhomogeneities formed during the gelation. Yet, the scattering patterns from the hydrogel and the solution are very similar, alluding to the low influence of the gelation on the local structure.

4 Conclusions

A combination of several scattering techniques and electron microscopy was used to characterize PEGylated polypeptides prepared *via* Michael-type addition of PEG to

denaturized fibrinogen. Upon urea removal, protein-protein interactions induced polypeptide self-assembly. The aggregates were elongated, and had a protein core of about 100 Å in diameter. PEGylation with branched PEG chains was more effective in preventing the aggregation. The improved understanding of the PEG-protein interactions in this system enabled the introduction of a structural model that was capable of predicting the relative location of each constituent in the final molecular assembly.

Acknowledgment The authors wish to thank Dr. Richard Heenan and Dr. Stephen King at ISIS facility of the Rutherford Appleton Laboratory (RAL, Chilton, UK) for their help with data collection and Dr. Daniel Dikovsky for his support with sample preparation. This research project has been supported by the European Commission under the Framework Program through the Key Action: Strengthening the European Research Area, Research Infrastructures. Contract no: RII3-CT-2003-505925. The authors gratefully acknowledge the financial support of the Israel Science Foundation (grant no. 1140/04).

References

1. Roberts MJ, Bentley MD, Harris JM. Chemistry for peptide and protein PEGylation. Adv Drug Delivery Res. 2002;54:459–76.
2. Krsko P, Libera M. Biointeractive hydrogels. Mater Today (Oxford). 2005;8:36–44.
3. Dikovsky D, Bianco-Peled H, Seliktar D. The effect of structural alterations of PEG-fibrinogen hydrogel scaffolds on 3-D cellular morphology and cellular migration. Biomaterials. 2006;27:1496–506.
4. Rizzi SC, Hubbell JA. Recombinant protein-co-PEG networks as cell-adhesive and proteolytically degradable hydrogel matrixes. Part I: development and physicochemical characteristics. Biomacromolecules. 2005;6:1226–38.
5. Almany L, Seliktar D. Biosynthetic hydrogel scaffolds made from fibrinogen and polyethylene glycol for 3D cell cultures. Biomaterials. 2005;26:2467–77.
6. An Q, Lei Y, Jia N, Zhang X, Bai Y, Yi J, et al. Effect of site-directed PEGylation of trichosanthin on its biological activity, immunogenicity, and pharmacokinetics. Biomol Eng. 2007;24:643–9.
7. Yu P, Zheng C, Chen J, Zhang G, Liu Y, Suo X, et al. Investigation on PEGylation strategy of recombinant human interleukin-1 receptor antagonist. Bioorg Med Chem. 2007;15:5396–405.
8. Prabhakaran M, Manjula Belur N, Acharya Seetharama A. Molecular modeling studies of surface decoration of hemoglobin by maleimide PEG. Artif Cells Blood Substit Immobil Biotechnol. 2006;34:381–93.
9. Svergun DI, Ekstroem F, Vandegriff KD, Malavalli A, Baker DA, Nilsson C, et al. Solution structure of poly(ethylene) glycol-conjugated hemoglobin revealed by small-angle X-ray scattering: implications for a new oxygen therapeutic. Biophys J. 2008;94:173–81.
10. Schmidt O, Mizrahi J, Elisseeff J, Seliktar D. Immobilized fibrinogen in PEG hydrogels does not improve chondrocyte-mediated matrix deposition in response to mechanical stimulation. Biotechnol Bioeng. 2006;95:1061–9.
11. Peled E, Boss J, Bejar J, Zinman C, Seliktar D. A novel poly(ethylene glycol)-fibrinogen hydrogel for tibial segmental defect repair in a rat model. J Biomed Mater Res, Part A. 2007;80A:874–84.
12. Shapira-Schweitzer K, Seliktar D. Matrix stiffness affects spontaneous contraction of cardiomyocytes cultured within a PEGylated fibrinogen biomaterial. Acta Biomater. 2007;3:33–41.
13. Dikovsky D, Bianco-Peled H, Seliktar D. Defining the role of matrix compliance and proteolysis in three-dimensional cell spreading and remodeling. Biophys J. 2008;94:2914–25.
14. Gonen-Wadmany M, Oss-Ronen L, Seliktar D. Protein–polymer conjugates for forming photopolymerizable biomimetic hydrogels for tissue engineering. Biomaterials. 2007;28:3876–86.
15. Nerem RM, Seliktar D. Vascular tissue engineering. Ann Rev of Biomed Eng. 2001;3:225–43.
16. West JL, Hubbell JA. Photopolymerized hydrogel materials for drug delivery applications. React Polym. 1995;25:139–47.
17. Tirelli N, Lutolf MP, Napoli A, Hubbell JA. Poly(ethylene glycol) block copolymers. Rev Mol Biotechnol. 2002;90:3–15.
18. Zisch AH, Lutolf MP, Hubbell JA. Biopolymeric delivery matrices for angiogenic growth factors. Cardiovasc Pathol. 2003;12:295–310.
19. Halstenberg S, Panitch A, Rizzi S, Hall H, Hubbell JA. Biologically engineered protein-graft-poly(ethylene glycol) hydrogels: a cell adhesive and plasmin-degradable biosynthetic material for tissue repair. Biomacromolecules. 2002;3:710–23.
20. Friedman M, Cavins JF, Wall JS. Relative nucleophilic reactivities of amino acids groups and mercaptide ions in addition reactions with a, b-unsaturated compounds. J Am Chem Soc. 1965;87:3672–82.
21. Debye P. Molecular-weight determination by light scattering. J Phys Colloid Chem. 1947;51:18–32.
22. Zimm BH. Apparatus and methods for measurment and interpretation of the angular variation of light scattering; preliminary results on polystyrene solutions. J Chem Phys. 1948;16:1099–116.
23. Glatter O, Kratky O. Small angle X-ray scattering. London: Academic Press; 1982.
24. Talmon Y. Cryogenic temperature transmission electron microscopy in the study of surfactant systems. Surfactant Sci Ser. 1999;83:147–78.
25. Pedersen JS. Form factors of block copolymer micelles with spherical, ellipsoidal and cylindrical cores. J Appl Crystallogr. 2000;33:637–40.
26. Pedersen JS. Analysis of small-angle scattering data from colloids and polymer solutions: modeling and least-squares fitting. Adv Colloid Interface Sci. 1997;70:171–210.
27. Pedersen JS, Gerstenberg MC. Scattering form factor of block copolymer micelles. Macromolecules. 1996;29:1363–5.
28. Seliktar D. Extracellular stimulation in tissue engineering. Ann N Y Acad Sci. 2005;1047:386–94.
29. Hall CE, Slayter HS. Fibrinogen molecule. Its size, shape, and mode of polymerization. J Biophys Biochem Cytol. 1959;5:11–6.
30. Upchurch GR Jr, Ramdev N, Walsh MT, Loscalzo J. Prothrombotic consequences of the oxidation of fibrinogen and their inhibition by aspirin. J Thromb Thrombolysis. 1998;5:9–14.
31. Bennion BJ, Daggett V. The molecular basis for the chemical denaturation of proteins by urea. Proc Natl Acad Sci. 2003;100:5142–7.
32. Hammouda B. A tutorial on Small-Angle Neutro Scattering from Polymers. Gaithersburg: National Institute of Standards and Technology; 1995.
33. Richtering W, Schmidt G, Linder P. Small-angle neutron scattering from a hexagonal phase under shear. Colloid Polym Sci. 1996;274:85–8.